37th European Rotorcraft Forum - Gallarate, Italy, 13-15 September 2011

Paper 218

Fast Free Wake: a Possible Approach to Real-Time Rotor Wake Simulation

F.Palo[2], R.Bianco Mengotti[1], F.Scorceletti[1], L.Vigevano[2]

[1] AgustaWestland, Flight Mechanics Dept., Cascina Costa di Samarate, Italy

[2] Dipartimento di Ingegneria Aerospaziale, Politecnico di Milano, Italy

Abstract

Accounting for wake-body interference effects in real-time simulations is still a challenge. To this aim the Fast Free Wake (FFW) model has been developed. It consists in a simple elaboration of the free-wake concept: vortex rings are released every certain time step from the rotor disk, and then they are free to move, interacting with all the other vorticity sources in the flow field without constraints. Wake deformation is accounted for by rings movement and diameter variation, while vorticity strength is directly related to the instantaneous rotor thrust value. The model has been developed, implemented, and then validated in hover, forward flight, vertical flight both In Ground Effect (IGE) and Out of Ground Effect (OGE). The computational efficiency of the model has been deeply investigated and the real-time running capability has been confirmed. The low computational cost required by FFW, together with its fair accuracy, makes the proposed model a valid tool for real-time flight mechanics simulations.

1 Introduction

The capability of modeling and representing the wake of a rotorcraft is essential to properly simulate most of the flight conditions, if not all. For conventional rotorcrafts, the main rotor wake typically affects the rotor itself, the fuselage, the empennages and the tail rotor, with impacts on performance, trim characteristics and manoeuvring flight. On tilt-rotors, the wake-body interaction is particularly important especially in hover and in low speed flight, with interesting interference phenomena in lateral and rearward flight. The accurate representation of the rotor wakes is still a challenge, due to the high computational power required by a complete free-wake model; notwithstanding the constant increase of computer power, it is still impossible to perform a complete free-wake simulation of helicopter rotor wakes in real time, in order to perform pilot-in-the-loop applications in simulator facilities.

The dynamic effect of the wake on rotor inflow has long been recognized. Finite-state dynamic wake models [1, 2, 3, 4] represent major advances in practical rotor wake simulation technology; however the hypothesis underlying these theories are not compatible with the simulation of certain flight regimes, for instance a descent flight approaching to the Vortex Ring State (VRS) condition. Recent developments on dynamic inflow models for descent flight make use of a series of vortex rings to create a non linear effect on rotor induced velocity, with the specific objective to simulating the VRS state [5, 6, 7, 8]. These approaches, being conceived as inflow models, represent only the near-wake and thus have not been utilized to investigate interference effects. A different approach, proposed by Horn *et al.* [9], sug-

gests to perform a complete and very accurate free-wake model calculation off-line, and then extract from the accurate simulations some parameters which are used to tune a very simplified free-wake real-time model, with stringent limitations both in spatial and temporal resolution. The drawback here is the need to tune the model for every analyzed configuration.

The present work reports a simple elaboration of the free-wake concept suitable to evaluate interference effects and computationally efficient so as to allow running in real-time. The two key element of the proposed approach, labeled Fast Free Wake (FFW) model, are vortex rings as elemental wake singularities and free movement of the ring themselves. The wake is considered as constituted by a set of vortex singularities, released from the tip path plane of the rotors with a certain frequency, which are free to move and to interact with other singularities in the field without constraints, since only the flight condition, and auto- and cross-induced velocities between singularities, regulate their motion. The singularity strength is determined from the rotor thrust and is kept constant during the time evolution of the wake. The number of vortex rings which represent the wake is limited by the user. These simplifications allow the FFW model to run in real-time on common desktop machines, with good margin for more complex simulations. The method, in fact, makes possible the introduction of different rotors, with simulation of mutual rotor interference, or the introduction of the ground effect, by means of a simple mirror plane technique, maintaining sufficient performance for real-time execution. It is important to underline that the model is presented here only as a wake representation, to be incorporated into a flight mechanics comprehensive code to evaluate interference effects. Its extension as inflow model is under development.

In the next sections, the model is described and validated in several conditions: hover, forward flight and descent flight, both in IGE and OGE conditions. The validation is both qualitative, in terms of velocity field and wake geometry, and quantitative, with particular attention to the descent flight in VRS regime and ground effect.

2 The FFW model

Vortex ring models have been used in the past to represent a prescribed wake [10, 11, 12], having the advantage of allowing for an analytical solution of the induced velocity field. They can however be employed also to model a free-wake: in the present FFW model the position and dimension of the vortex rings are determined only by free stream conditions and the auto and mutual influences between vortical singularities. Each ring is released from the rotor disk at a given time interval $\Delta\tau$; it is displaced with its local velocity until it becomes too "old" – when its influence on the field can be considered negligible – and it is eliminated. A full interaction between all rings present in the field is retained, although a simplified model is also introduced where the influence of a ring located further than a given distance – typically twice the rotor radius – is neglected.

The adopted general free-wake procedure is the following:

1. A new vortex ring is released, corresponding to the circumference of rotor tip path plane, with given intensity, directly proportional to current rotor thrust. A set of control points is associated to the ring. The total number of singularities in the vortex system, denoted with N, is kept constant by eliminating the "older" ring from the wake.

2. The local velocity at the ring control points is computed, accounting for free stream contribution and the velocity induced by the whole vortex system.

3. Each ring is displaced and resized by moving the control points with local velocity, but its circular shape is not modified.

4. The geometrical description of the rings is updated after the movement. The wake deformation is continued by repeating steps 2-4.

5. When the time elapsed reaches the value $\Delta\tau$, the procedure is restarted from step 1.

The wake shedding will of course have a transient where the number of singularities will increase to reach the value N.

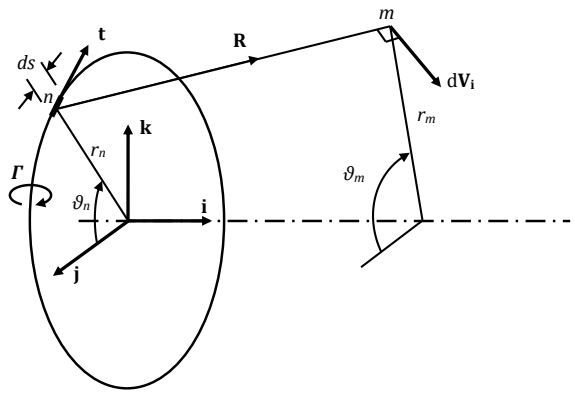

Figure 1: Geometrical representation of a vortex ring

2.1 Induced velocity

The induced velocity, due to an infinitesimal vortex element, is provided by the Biot-Savart law:

$$d\mathbf{V}_i = \frac{\Gamma}{4\pi}\frac{ds\,\mathbf{t}\times\mathbf{R}}{|\mathbf{R}|^3}\ . \tag{1}$$

For the vortex ring geometry, the unit vector $\mathbf{t}$, the ring segment ds and the vector $\mathbf{R}$ connecting the ring segment to the sample point, are illustrated in fig. 1 and defined as:

$$\begin{cases} \mathbf{t} = -\sin\vartheta_n\mathbf{j} + \cos\vartheta_n\mathbf{k} \\ ds = r_n d\vartheta_n \\ \mathbf{R} = x_m\mathbf{i} + (r_m\cos\vartheta_m - r_n\sin\vartheta_n)\,\mathbf{j} \\ \qquad\quad + (r_m\sin\vartheta_m - r_n\sin\vartheta_n)\,\mathbf{k} \end{cases}\ , \tag{2}$$

where r_n is the ring radius, ϑ_n, ϑ_m are the azimuthal coordinates of, respectively, a point n on the ring and the sample point m where the induced velocity is computed, and x_m, r_m are the axial and radial coordinates of point m.

Integrating eq. (1) along the complete ring, we obtain the following expression for the axial and radial velocity components:

$$u_{mn} = \frac{\Gamma}{4\pi}\int_0^{2\pi} \frac{r_n - r_m\cos(\vartheta_m - \vartheta_n)}{\left[x_m^2 + r_m^2 + r_n^2 - 2r_m r_n\cos(\vartheta_m - \vartheta_n)\right]^{3/2}} d\vartheta_n\ , \tag{3}$$

$$v_{mn} = \frac{\Gamma}{4\pi}\int_0^{2\pi} \frac{(x_n - x_m)\cos(\vartheta_n)}{\left[x_m^2 + r_m^2 + r_n^2 - 2r_m r_n\cos(\vartheta_m - \vartheta_n)\right]^{3/2}} d\vartheta_n\ . \tag{4}$$

Introducing the non dimensional axial and radial coordinates x and r as:

$$x = \frac{x_m}{r_n}, \qquad r = \frac{r_m}{r_n}, \tag{5}$$

it finally results:

$$u_{mn} = \frac{\Gamma}{2\pi r_n\sqrt{x^2 + (r+1)^2}}\left(K(k) - \left(1 + \frac{2(r-1)}{x^2 + (r-1)^2}\right)E(k)\right)\ , \tag{6}$$

$$v_{mn} = \frac{-\Gamma x/r}{2\pi r_n\sqrt{x^2 + (r+1)^2}}\left(K(k) - \left(1 + \frac{2r}{x^2 + (r-1)^2}\right)E(k)\right)\ , \tag{7}$$

where $K(k)$ and $E(k)$ are complete elliptic integrals of the first and second kind, and k is defined as:

$$k = \sqrt{\frac{4r}{x^2 + (r+1)^2}} \equiv \sin\phi\ . \tag{8}$$

Equations (6),(7) may become singular: for instance the axial velocity component is singular

for $x = 0$ and $r = 1$, on the ring itself; the radial component is singular also for $r = 0$, on the ring axis. Singularity is avoided by imposing vortex core of constant radius $\varepsilon = 0.05 r_n$, where the velocity is linearly varying. An identical approach is considered at the ring axis.

The elliptic integrals, given by [13]:

$$K(k) = \int_0^{\pi/2} \frac{1}{\sqrt{1 - k^2 \sin^2 \alpha}} d\alpha \ , \qquad (9)$$

$$E(k) = \int_0^{\pi/2} \sqrt{1 - k^2 \sin^2 \alpha} d\alpha \ , \qquad (10)$$

can be computed in advance using numerical quadrature and stored as tables, function of the parameter k. For $\phi(k) \to 90°$, when the integrals become singular, it is possible to use the asymptotic expressions:

$$K(k) = \ln\left(4/\cos\left(\phi\right)\right) \ , \qquad (11)$$

$$E(k) = 1 + \frac{1}{2}\left(K(k) - \frac{1}{1.2}\right)\cos^2\left(\phi\right) \ . \qquad (12)$$

To deal with IGE, the classical mirror image technique [14] can be adopted.

2.2 Ring movement

While moving with their local velocity, the vortex rings may change their dimensions and orientation, with the only limitation of remaining perfectly circular, in order to exploit the analytical solution for the induced velocity. Each ring is marked with four control points (fig. 2), located along perpendicular rays at radial distance from the ring axis given by $\varepsilon_r r_n$, where r_n is the present ring radius and ε_r, $0 < \varepsilon_r < 1$, is an empirical coefficient which is set to the value 0.7. The ring is uniquely determined in a global reference system by the location of its center, its radius and a set of unit vectors which describe its inclination in the given reference system, as show in fig. 3.

Induced velocity components are evaluated at the control points, making use of equations (6),(7) and measured in an inertial reference frame. The control points displacements are computed through a simple forward Euler scheme with time Δt. Once the updated location of the four control points is computed, the location of the ring center and its radius are simply obtained as:

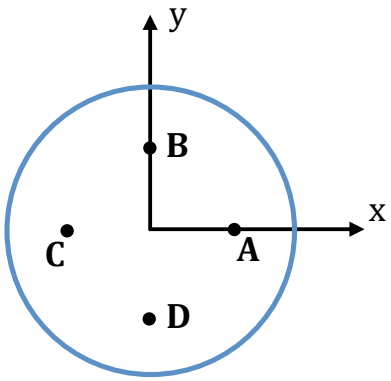

Figure 2: Location of ring control points

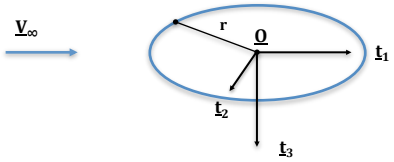

Figure 3: Ring local reference frame

$$\mathbf{O} = \frac{\mathbf{A} + \mathbf{B} + \mathbf{C} + \mathbf{D}}{4} \ , \qquad (13)$$

$$r_n = \frac{1}{4 \cdot \varepsilon_R}\left(|\mathbf{OA}| + |\mathbf{OB}| + |\mathbf{OC}| + |\mathbf{OD}|\right) \ . \qquad (14)$$

Finally, the unit vectors which describe the ring orientation are recomputed as:

$$\mathbf{t}_1 = \frac{\mathbf{CA}}{|\mathbf{CA}|} \ , \mathbf{t}_3 = \frac{\mathbf{CA} \times \mathbf{BD}}{|\mathbf{CA} \times \mathbf{BD}|} \ , \mathbf{t}_2 = \mathbf{t}_3 \times \mathbf{t}_1 \ . \qquad (15)$$

2.3 Vortex strength and release time

A constant value of the circulation is associated to the vortex singularity at the instant of its release, as:

$$\Gamma = 4 k_\Gamma k_p \frac{T}{\rho V_{tip} A \sigma} \ , \qquad (16)$$

with T instantaneous value of the rotor thrust, $V_{tip} = \omega R$ rotor tip speed, R rotor radius, A rotor area and σ rotor solidity; the coefficient k_Γ is an empirical scale factor, determined from comparison studies with a classical free-wake vortex lattice model, thus assuming the value $k_\Gamma = 1.2$. The coefficient k_p is a second scaling factor, related to the fact that the vortex rings are not released at every blade passage, but with a periodicity which aims at having a reasonable ring distribution within the wake. From numerical experiments, it has been found that the optimal wake "density" is achieved with four vortex rings within the distance of one rotor radius. The coefficient k_p is obtained as:

$$k_p = \frac{R}{u_{ad} + |\mathbf{V}_\infty|} \ , \tag{17}$$

where $u_{ad} = \sqrt{T/2\rho A}$ is the induced velocity in hover from momentum theory; k_p is a reasonable estimation of the time needed to cover a distance equal to R.

The release time interval $\Delta\tau$ is closely linked to k_p, inasmuch that four rings shall be located within one rotor radius from the tip path plane; therefore we select $\Delta\tau = \frac{k_p}{4}$.

2.4 Computational efficiency

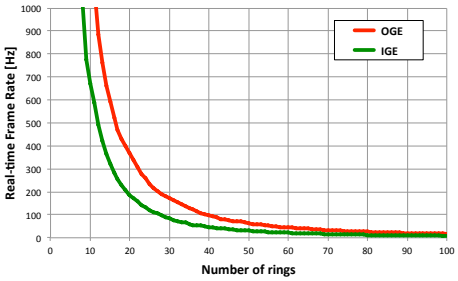

Figure 4: Computational requirements in hover IGE and OGE.

The computational efficiency of the proposed algorithm has been evaluated introducing a quantitative index, labeled frame-rate: it corresponds to the reciprocal of the CPU time needed to perform one step of wake movement for a wake made of N singularities.

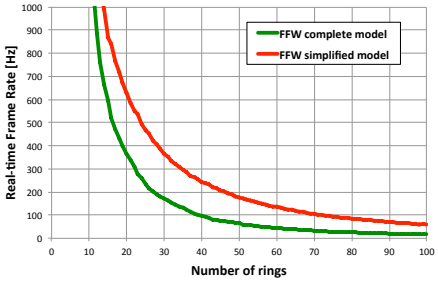

(a) *OGE*

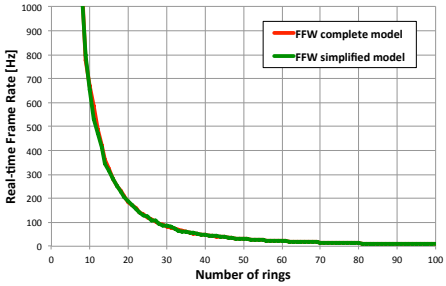

(b) *IGE*

Figure 5: Computational requirements in hover using the full and simplified FFW models.

In figure 4 are reported the frame-rate values, as function of the number N of the vortex rings in the field, for a test case in hover conditions, both IGE and OGE. Quite obviously the IGE condition, performing more calculations because of the mirror image technique, has the lowest frame rate for a given N. Since the wake may usually be well represented using $20 < N < 30$, the achieved computational cost is compatible with a real-time analysis. Since the computational burden depends only from the value of N, similar results may be found for other flight conditions.

A simplified method has been evaluated, in which the influence region of each singularity is limited to a distance of $2R$ from its axis. In OGE condition (fig. 5a) the simplified approach improves the frame-rate, still predicting a wake shape very close to that of the original method. In IGE (fig. 5b), on the contrary, no improvement can be noticed, because the presence of the ground makes the wake much more compact.

Since the method that accounts for the full influence of the wake elements is compatible with a real-time analysis, it is retained for the validation activity described in the next section.

3 Model validation

The following sections present a thorough validation of the FFW model in the most significative flight regimes: hover and forward flight, both in IGE and OGE conditions, climb and descent flight. Results in terms of wake geometry and velocity fields are compared against experimental data and computations from other models found in the literature.

3.1 Hover OGE

In this section a description of the results obtained for hovering flight out of ground effect is presented. The first test case that has been considered refers to the model rotor investigated by Boffadossi and Crosta [15]. The rotor has four rectangular blades, with a radius of 0.8m, and a solidity of 0.0955. Experimental tests were performed at $C_t/\sigma = 0.075$. Hot wire measurements were taken in a radial plane at sixty spanwise locations in the range $0.288 < r/R < 1.025$ at several z/R axial distances and compared with numerical results gathered from a free-wake vortex-lattice method.

The FFW simulation is characterized by a temporal integration step Δt equal to 1/10 of the vortex release time, $\Delta\tau$, and lasts 600 Δt. After 200 Δt the vortex is considered dissipated so that, after the initial transient, the flow field will be always populated by 20 vortex rings.
For comparison purpose with experimental data at a distance z/R = -0.6 downstream the rotor, the mean induced velocity is evaluated by averaging over the 100 last temporal integration steps of the simulation, when the wake is already fully developed. Results are presented in Figure 6 using various values of k_Γ, to verify that the choice of $k_\Gamma = 1.2$ was justified.
In fact, the trend of the average velocity profile for $k_\Gamma = 1.2$ fits the experimental curve with a good approximation for values of r/R greater than 0.8. In the inner zone of the wake the agreement is not as good, because of the model inability to describe the inner wake vortices, which are not taken into account by the FFW theory. A possible solution, under investigation, is to release from he rotor disk additional internal rings, coaxial to the outer ones, with smaller radius and lower intensity. It should however be noticed that the choice of $k_\Gamma = 1.2$ is the best compromise also for the inner zone: the area under the velocity profile, and therefore the average velocity on the considered plane, is closest to that obtained experimentally.
Interestingly, the FFW model, for a radial distance grater than $x/R = 0.85$, provides results closer to experimental ones than those obtained by Boffadossi and Crosta with a vortex-lattice method.

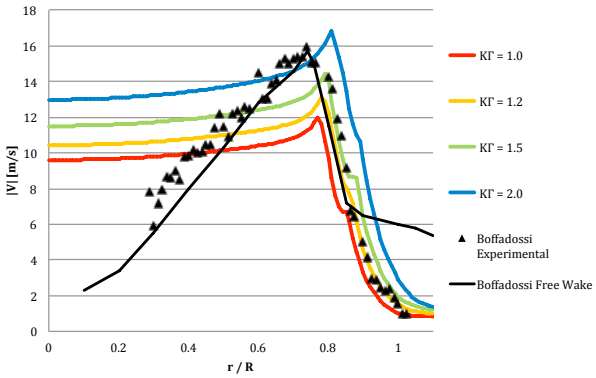

Figure 6: Mean induced velocity modulus at a distance of $z/R = 0.6$ at various k_Γ and $\varepsilon_R = 0.7$, compared with Boffadossi-Crosta numerical and experimental results

The second considered test case refers to the seven blade CH53E main rotor, with radius R = 12m and solidity $\sigma = 0.121$, for the condition $C_t/\sigma = 0.0963$. The wake geometry obtained with FFW has been compared qualitatively with the free-wake results reported in [12]. FFW model parameters are still $k_\Gamma = 1.2$ and $\varepsilon_R = 0.7$, and the simulation time step and duration are exactly the same as for the previous case. In Figure 7b the longitudinal velocity field is compared against the superimposed black curve representing the free-wake geometry obtained by Leishman. In the rotor proximity, up to a downstream distance of 1.5R, the FFW velocity field has a good qualitative match with that obtained with a classic free-wake method. In the far wake, FFW

tries to follow the aperiodic behavior, which is correctly modeled by the free-wake method; in fact at those distances the vortex ring radius increases, as noticed in Figure 7a, before being canceled to simulate dissipation.

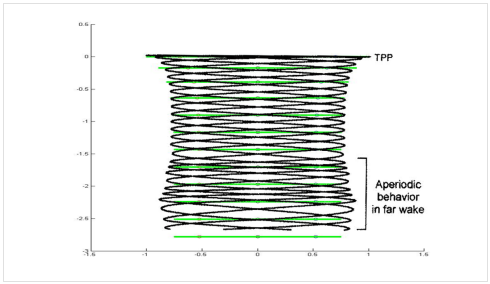

(a) *FFW Rings geometry*

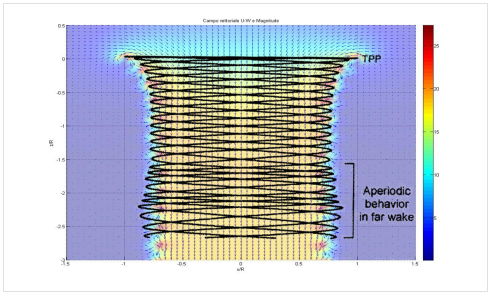

(b) *FFW Longitudinal Velocity Field*

Figure 7: FFW in hover OGE compared against Leishman free-wake geometry

Finally, in Figure 8 a comparison of the computed wake contraction for the CH53E main rotor against Landgrebe [16] theoretical tip vortex geometry, is reported. A good agreement is confirmed.

3.2 Hover IGE

In this section results for hovering flight in ground effect are shown. The CH53E rotor at a height $h = 37ft$ from the ground is simulated, with the same parameters and time discretization used for the hover OGE validation. The mean velocity at 20 distances from the ground, between 0 and 12ft, is evaluated averaging on the last 100 temporal steps and is compared in figure 9 with the experimental data from reference [17]. The plot reports also the minimum and maximum values of the computed velocity. The FFW result trends are quite in agreement with the experimental ones. The corresponding computed wake geometry is shown in figure 10.

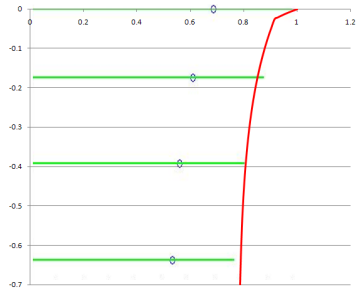

(a) *FFW Rings geometry*

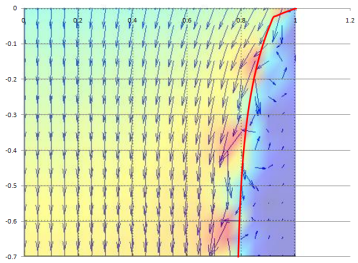

(b) *FFW Velocity Field*

Figure 8: Wake contraction for FFW in Hover OGE compared against Landgrebe tip vortex geometry (red line)

Furthermore, the ground effect factor $f_g = \frac{|\mathbf{u}_{IGE}|}{|\mathbf{u}_{OGE}|}$ is calculated for the CH53E rotor and for a AW139 main rotor model; the average velocity on the rotor disk is again obtained by averaging on 100 time steps and performing a numerical integration over the rotor surface. The computed values of f_g are compared with experimental data from Light [18] and with the empirical models described in [19]. The agreement of FFW results with empirical and experimental ones is satisfactory.

3.3 Axial climb and descent flight

In this section the behavior of the model in axial climb and descent flight is analyzed, considering the CH53E main rotor. Particular attention is addressed to check the model capability in simulating the condition of vortex ring state (VRS). Simulations have been performed for axial speeds between $10m/s$ and $-60m/s$ with the same computational parameters used during hover analysis. Results are compared with the solution of the extended Momentum Theory (MT), with theoretical and experimen-

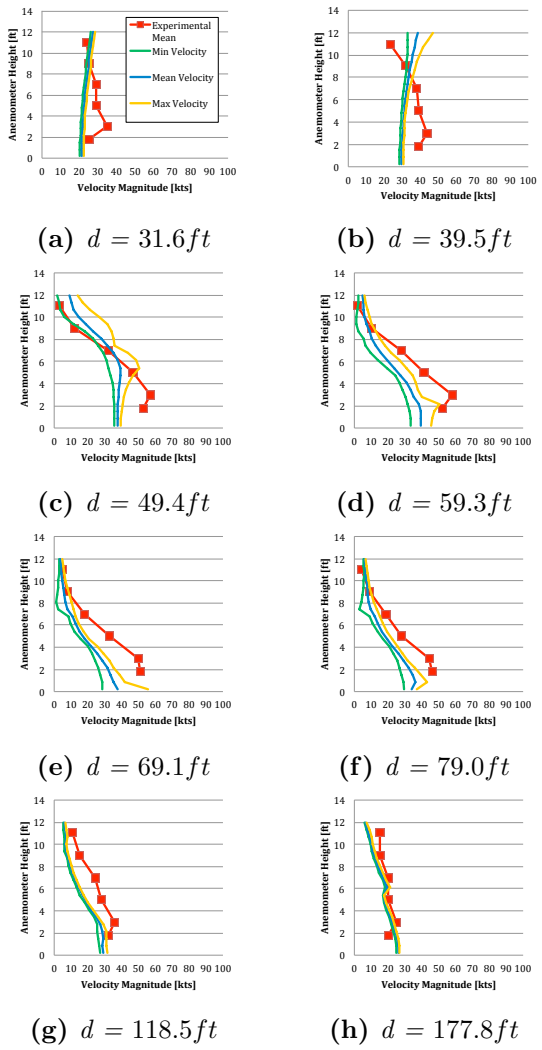

(a) $d = 31.6ft$ **(b)** $d = 39.5ft$

(c) $d = 49.4ft$ **(d)** $d = 59.3ft$

(e) $d = 69.1ft$ **(f)** $d = 79.0ft$

(g) $d = 118.5ft$ **(h)** $d = 177.8ft$

Figure 9: CH53E Main Rotor IGE at $h = 37ft$, induced velocity at various distances d from rotor axes

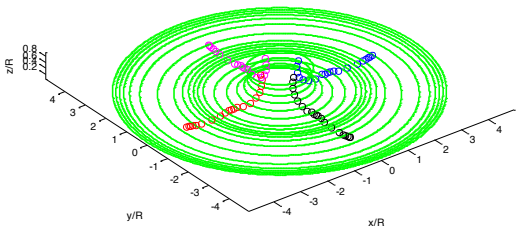

Figure 10: FFW wake geometry in hover IGE at $h = 37ft$

tal data gathered at the ONERA [20] about the VRS regime, and with Leishman [12] free-wake geometry.

Initially a qualitative validation, comparing the obtained FFW wake geometry with classical free-wake results reported in [12], is carried out. In figure 12 is possible to see the velocity fields

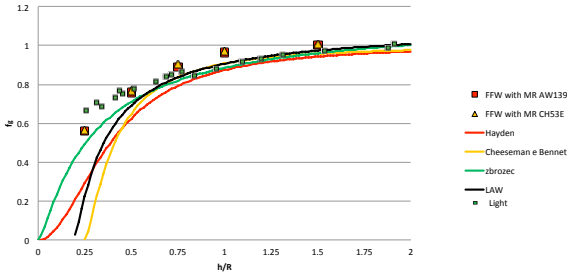

Figure 11: FFW Ground Effect Factor f_g in Hover for CH53E Main Rotor and AW139 Main Rotor compared against theoretical models and experimental results

of the FFW model at some significant descent speed, compared with the free-wake geometry represented by a black solid line. The general behavior is correctly predicted, except for the wake instabilities detected by the classical free-wake model.

For a quantitative comparison with the extended Momentum Theory curves, and the theoretical and experimental results by ONERA [20], the FFW average velocity on the rotor disk is obtained at various axial distances d immediately downstream of the rotor, up to $d = 0.25R$. The averaging process is done integrating on effective wake area. Figure 13 shows that FFW results have a good correspondence with the extended Momentum Theory ones, but are slightly underestimated in absolute value with respect to ONERA theory. At low rate of descent the curve closest to the theoretical one is that at a distance $d = 0.25R$, while at higher rate the best match is obtained on the rotor disk($d = 0$).

Finally, the good agreement of the FFW model with the extended Momentum Theory is demonstrated also in terms of required power in figure 14. We can observe that FFW is qualitatively capable of modeling the phenomenon of VRS, and can also identify the power settling zone in which the required power is increasing rather than decreasing with respect to the descent velocity.

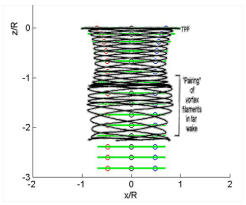

(a) $v_z = 4m/s$ - *Very Low rate of descent*

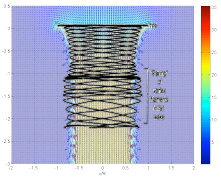

(b) $v_z = 4m/s$ - *Very Low rate of descent*

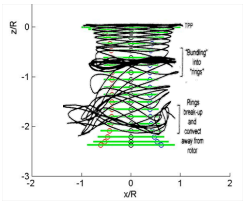

(c) $v_z = 10m/s$ - *Low rate of descent*

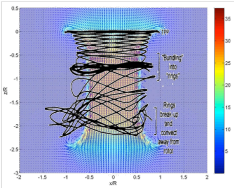

(d) $v_z = 10m/s$ - *Low rate of descent*

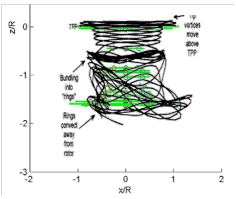

(e) $v_z = 14m/s$ - *High rate of descent*

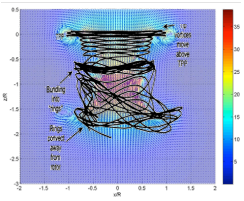

(f) $v_z = 14m/s$ - *High rate of descent*

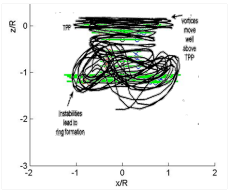

(g) $v_z = 16m/s$ - *Incipient VRS*

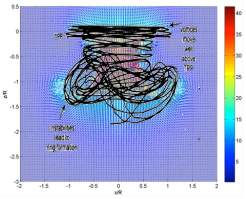

(h) $v_z = 16m/s$ - *Incipient VRS*

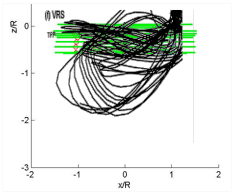

(i) $v_z = 20m/s$ - *VRS*

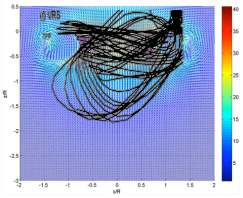

(j) $v_z = 20m/s$ - *VRS*

Figure 12: Comparison between FFW geometry and velocity field and free-wake (black lines) in axial descent

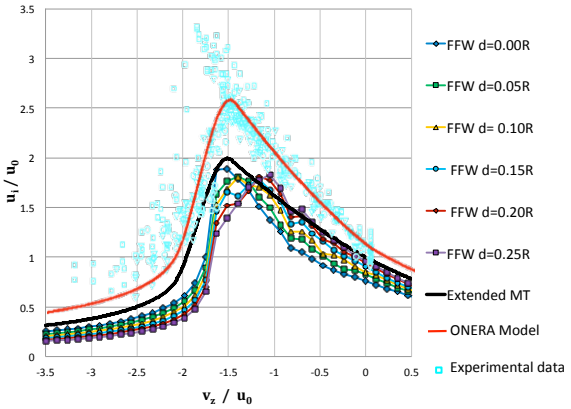

Figure 13: Normalized average induced velocity in axial descent for FFW model at various distances from rotor plane, compared to extended Momentum Theory , ONERA Model and experimental results

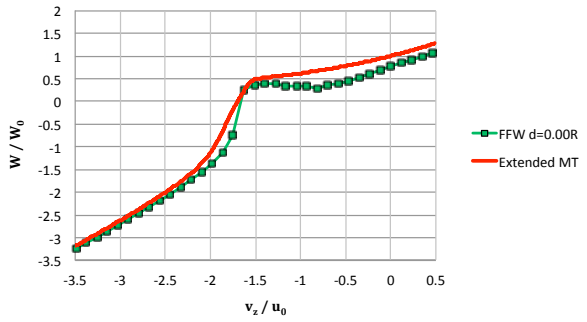

Figure 14: Normalized power required in axial descent for FFW model and extended Momentum Theory

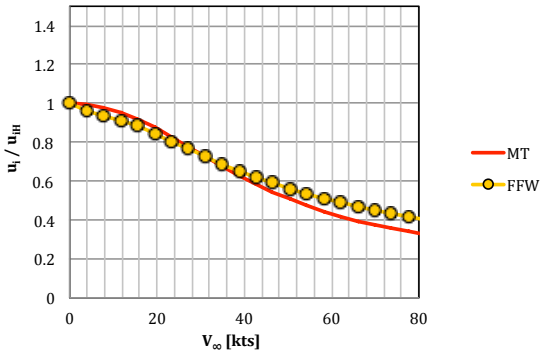

Figure 15: Normalized average induced velocity in forward flight for FFW and Momentum Theory

3.4 Forward flight OGE

The FFW model is validated in forward flight conditions simulating the CH53E main rotor, with usual model and time discretization parameters.

To perform a quantitative comparison with momentum theory, the mean velocity on the rotor disk has been calculated, integrating the velocity distribution on the disk surface. Results in term of normalized velocity are reported in Figure 15, where a good agreement can be observed.

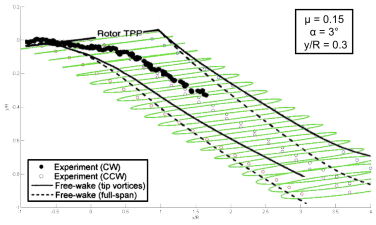

(a) *Wake geometry at* $\mu = 0.15$

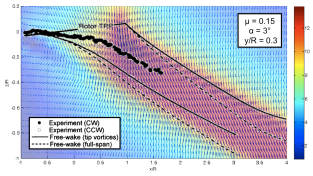

(b) *Velocity field at* $\mu = 0.15$

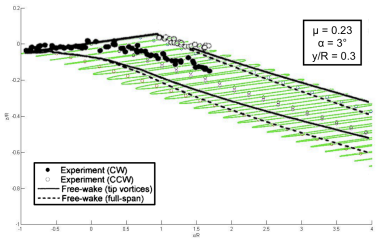

(c) *Wake geometry at* $\mu = 0.23$

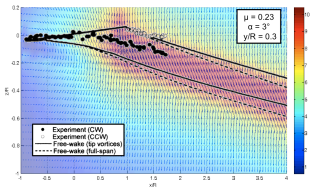

(d) *Velocity field at* $\mu = 0.23$

Figure 16: Comparison between FFW, experiments and free-wake (black lines) in OGE forward flight on longitudinal plane

Figure 16 shows longitudinal slices of the FFW wake geometry and induced flow-field for $\mu = 0.15$ and $\mu = 0.23$, on a plane normal to the rotor disk at a distance of 0.3R from rotor disk axis. Results are compared with free-wake and experimental ones from Ghee and Elliot [21]. In order to reduce velocity peaks on the external boundary of the wake, which could result in unrealistic local velocity fluctuations affecting the rotorcraft aerodynamic surfaces, the desingularization core ϵ_R has been increased to 0.1 in this simulation. Good qualitative agreement with free-wake and experiments is found both for longitudinal and transverse wake shape.

3.5 Forward flight IGE

The rotor used to analyze the qualitative behavior of the FFW model in forward flight IGE, is the five bladed AW139 model rotor considered by Biava *et* al. for RANS calculations [22], with radius $R = 0.9m$, solidity $\sigma = 0.1025$ and $C_t/\sigma = 0.1$. The FFW simulation parameters, time discretization, and simulation duration are the same used in previous validations, but the number of rings in the flow fields is augmented to 30, to have a correct match with the computed RANS velocity field. The rotor height above ground has been fixed to $2R$, the rotor angle of attack is $\alpha = -5°$, and the range of advance ratio considered is $0.02 < \mu < 0.07$. In Figure 17 is possible to see the longitudinal FFW velocity fields compared with RANS vorticity contours, represented by the black solid lines. FFW wake geometries show a good qualitative mach with RANS ones.

Finally, in figure 18 is reported the normalized induced velocity variation with forward speed at several altitudes on ground, obtained with FFW and with Heyson's relations. Through theoretical and experimental studies, based mainly on wind tunnel tests, Heyson obtained a semi-empirical expression for the calculation of the wake induced speed in forward flight in ground effect [23] [24]. In particular, the expression for normalized induced velocity at the center of the rotor is:

$$\frac{u_i}{u_{iH}} = \sqrt{\cos(\chi)} + \frac{\Delta u}{u_{iH}} \,, \tag{18}$$

where $\chi = V_\infty / u_{i0}$ is the wake skew angle, u_{i0} is the induced velocity at rotor center in OGE, u_{iH} the induced velocity in hover and Δu the induced velocity only due to ground influence, function of wake skew angle, wind tunnel chamber dimension, and of Heyson's correction factor.
Figure 18 shows that the curves trend is well predicted by the FFW model, although some quantitative differences can be observed.

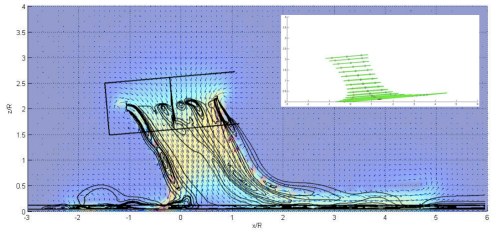

(a) $\mu = 0.02$

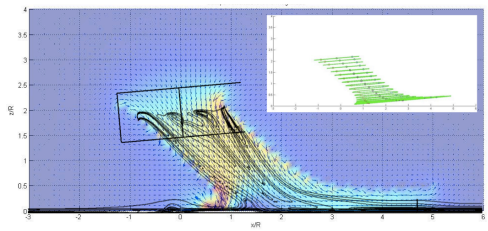

(b) $\mu = 0.047$

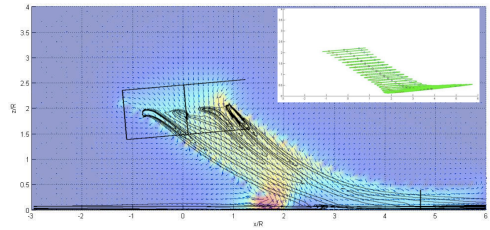

(c) $\mu = 0.058$

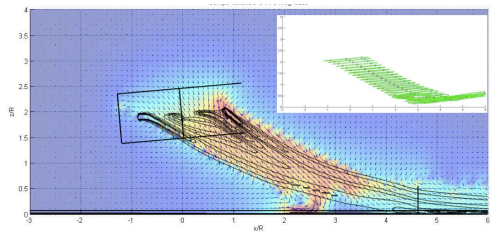

(d) $\mu = 0.07$

Figure 17: Longitudinal velocity field in IGE forward flight compared with RANS (black solid lines)

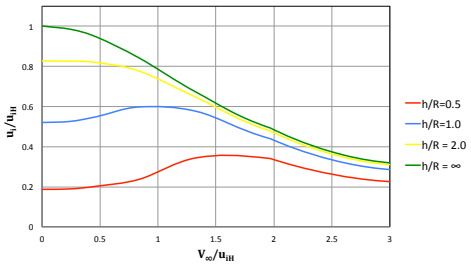

(a) *Heyson*

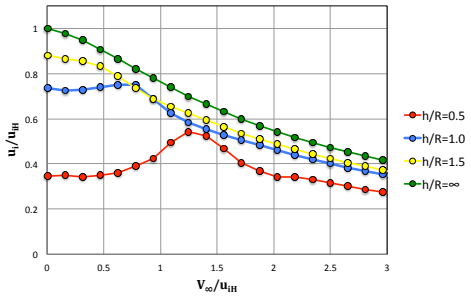

(b) *FFW*

Figure 18: Normalized induced velocity variation with forward speed in IGE regime

4 Conclusions

A new wake model to approach real-time simulation has been presented. The FFW model has been developed adopting a free-wake concept, but simplifying the vorticity representation, in order to optimize the computational cost. The model has been described and then thoroughly validated in several significative flight conditions.

The quality of the model has emerged in all flight conditions from both qualitative and quantitative standpoints, always giving a good simulation of the physical phenomenon and presenting a good agreement with experimental data or numerical results achieved with more sophisticated theoretical models. In particular, the model can adequately reproduce and predict the regime of Vortex Ring State, at which all released ring vortex correctly concentrate at the rotor disk. In regard with forward flight IGE, the model manages to correctly reproduce the formation of a pseudo-toroidal vortex in front of the rotor, of course not open at the infinity, but closed because of the vortex ring shape.

It is important to notice that the present model has been developed to obtain a flexible tool able to perform fast analysis, compatible with real-time simulations, but do not pretend to replace experimentation or the more advanced tools, such as RANS solvers or free-wake codes, which are certainly able to describe the physical phenomenon with a level unattainable by the FFW model, but at a significantly higher cost. On the other hand, the FFW model is certainly a flexible tool, able to allow quick and accurate analysis in all flight conditions, as shown in the validation section. The degree of accuracy achieved can be considered sufficient to perform flight mechanics analysis.

References

[1] Pitt, D.M., and Peters, D.A., Theoretical Prediction of Dynamic Inflow Derivatives, *Vertica*, Vol. 5 (1), pp. 21-34, 1981.

[2] Peters, D.A., He, C.J., and Boyd, D.D., A Finite-State Induced-Flow Model for Rotors in Hover and Forward Flight, *Journal of the American Helicopter Society*, Vol. 34 (4), pp. 5-17, 1989.

[3] Peters, D.A., and He, C.J., Correlation of Measured Induced Velocities with a Finite-State Wake Model, *Journal of the American Helicopter Society*, Vol. 36 (3), pp. 59-70, 1991.

[4] Peters, D.A., and He, C.J., Finite State Induced Flows Models Part II: Three-Dimensional Rotor Disk, *Journal of Aircraft*, Vol. 32 (2), 1995.

[5] Chen, C., and Prasad, J.V.R., A Simplified Inflow Model of a Helicopter in Forward Descent, *43rd AIAA Aerospace Science Meeting and Exhibit*, Reno, Nevada, AIAA 2005-622, 2005.

[6] Chen, C., and Prasad, J.V.R., Simplified Rotor Inflow Model for Descent Flight, *Journal of Aircraft*, Vol. 44 (3), pp. 936-944, 2005.

[7] Basset, P.-M., Chen, C., Prasad, J.V.R., and Kolb, S., Prediction of Vortex Ring State, *Journal of the American Helicopter Society*, Vol. 56, pp. 022001/1-02201/14, 2011.

[8] Brand, A., Dreier, M., Kisor, R., and Wood, T., The Nature of Vortex Ring State Boundary of a Helicopter in Descending Flight by Simulation, *Journal of the American Helicopter Society*, Vol. 53 (2), pp. 139-151, 2008.

[9] Horn, J.F., Bridges, D.O., Wachspress, D.A., and Rani, S.L., Implementation of a Free-Vortex Wake Model in Real-Time Simulation of Rotorcraft, *Journal of Aerospace Computing, Information and Communication*, Vol. 3, pp. 93-114, 2006.

[10] Gibson, I.S., and Lewis, R. I., Ducted Propeller Analysis by Surface Vorticity and Actuator Disk Theory, *Symposium on Ducted Propellers*, R.N.I.A., Paper No.1, 1973.

[11] Lewis, R.I., *Vortex Element Methods for Fluid Dynamic Analysis of Engineering System*, Cambridge University Press, Cambridge (UK), 1991.

[12] Leishman, J.G., *Principles of Helicopter Aerodynamics*, Cambridge Aerospace Series, NewYork, 2006.

[13] Dwight, H. B., (1963). *Tables of integrals and other mathematical data*, Macmillan, New York, 1963.

[14] Padfield G.D., *Helicopter Flight Dynamics*, Blackwell Science, Oxford, 2000.

[15] Boffadossi M., Crosta G., Experimental Investigation and Numerical Study of a Helicopter Rotor Model, *XX AIDAA Conference*, Milano, June 29 - July 3, 2009.

[16] Landgrebe A.J., The Wake Geometry of Hovering Helicopter Rotor and its Influence on Rotor Performance, *J. of the American Helicopter Society*, 17(4), pp. 3-15, 1972.

[17] Ferguson, S.W., *Rotorwash Analysis Handbook - Volume 1: Development and Analysis*, System control Technology Inc, Arlington VA, June 1994.

[18] Light, J. S., Tip Vortex Geometry of a Hovering Helicopter Rotor in Ground Effect, *Journal of the American Helicopter Society*, Volume 38, No. 2, April 1993.

[19] Johnson, W., NASA Design and Analysis of Rotorcraft, *NASA/TP-2009-215402*, Ames Research Center, Moffett Field, California, December 2009.

[20] Taghizad, A., Jimenez, J., Binet, L., and HeuzÈ, D., Experimental and Theoretical Investigations to Develop a Model of Rotor Aerodynamics Adapted to Steep Descents, *American Helicopter Society 58th Annual Forum*, MontrÈal, Canada, June 11-13, 2002.

[21] Ghee, T.A., and Elliot, J.W., The Wake of a Small-Scale Rotor in Forward Flight

Using Flow Visualization, *Journal of the American Helicopter Society*, 40(3), pp. 52-65, July 1995.

[22] Biava, M., Thomopoulos, A., and Vigevano, L., Computational Assessment of Flow Breakdown in Closed Section Model Rotor Tests, *37th European Rotorcraft Forum*, Gallarate (VA), Italy, Sept. 2011.

[23] Heyson, H.H., Ground Effect for Lifting Rotors in Forward Flight, *NASA TN D-234*, Washington, May 1960.

[24] Heyson, H.H., Jet-Boundary Correction for Lifting Rotors Centered in Rectangular Wind Tunnels, *NASA TR R-71*, Washington, 1960.